Journal of Materials Chemistry B

Accepted Manuscript

ROYAL SOCIETY OF CHEMISTRY

www.rsc.org/materialsB

Journal of Materials Chemistry B

Cite this: DOI: 10.1039/c0xx00000x

PAPER

www.rsc.org/xxxxxx

Targeted CT imaging of human hepatocellular carcinoma using low-generation dendrimer-entrapped gold nanoparticles modified with lactobionic acid†

Yiyun Cao,[a§] Yao He,[b§] Hui Liu,[c] Yu Luo,[c] Mingwu Shen,[c] Jindong Xia,*[b] Xiangyang Shi*[ac]

Received (in XXX, XXX) Xth XXXXXXXXX 20XX, Accepted Xth XXXXXXXXX 20XX
DOI: 10.1039/b000000x

Development of cost-effective nanoscale contrast agents for targeted tumor CT imaging still remains a great challenge. Here, we report the synthesis of dendrimer-entrapped AuNPs (Au DENPs) using generation 2 (G2) poly(amidoamine) dendrimers pre-modified with fluorescein isothiocyanate *via* a thiourea linkage and lactobionic acid (LA) *via* a polyethylene glycol (PEG) spacer as templates. The formed Au DENPs were characterized *via* different techniques and were used as a nanoprobe for targeted CT imaging of hepatocellular carcinoma (HCC). We show that the LA-modified Au DENPs with a mean Au core size of 1.8 nm are water-dispersible, colloidally stable under different temperature (4-50 ^{o}C) and pH (5-8) conditions, and cytocompatible in the studied concentration range. Flow cytometry results reveal that the LA-Au DENPs are able to specifically target HepG2 cells (a human HCC cell line) overexpressing asialoglycoprotein receptors *via* a receptor-mediated targeting pathway. Importantly, the developed LA-Au DENPs are able to be used as a nanoprobe for targeted CT imaging of HepG2 cells *in vitro* and the xenografted tumor model *in vivo*. With the demonstrated organ compatibility, the developed LA-Au DENPs using low-generation dendrimers as templates may hold great promise to be used as a highly efficient and cost-effective nanoprobe for targeted CT imaging of HCC.

Introduction

Computed tomography (CT) has been identified as one of the most widespread molecular imaging technologies due to its high density and spatial resolution, cost effectiveness, deep penetration capability, and facile 3-dimensional imaging reconstruction technique.[1, 2] For high-quality CT imaging of soft tissues, contrast agents are normally required. Conventionally used CT contrast agents are iodine-based small molecules (e. g., Omnipaque), suffering problems of short imaging time due to their fast clearance by kidney, renal toxicity at a relatively high concentration,[3] and non-specificity. It is essential to develop various novel CT contrast agents to overcome the above shortcomings.

Nanotechnology has made a significant contribution to the development of various nanoscale contrast agents for CT imaging applications. Various nanoparticulate contrast agents such as bismuth sulfide nanoparticles (NPs),[4-7] lanthanide-doped BaYbF5 upconversion nanoprobes,[8] lutetium-based nanoparticulate contrast agents,[9] ytterbium-based NPs,[10, 11] tantalum oxide NPs,[12] and gold NPs (AuNPs)[13] have been used for CT imaging of different biological systems. Among the different types of nanoscale CT contrast agents, AuNPs have been paid a great deal of attention thanks to their better X-ray attenuation property than iodinated CT contrast agents, chemical stability, and good biocompatibility after surface functionalization.[1, 14-17]

To form stable and biocompatible Au colloids, various ligand molecules have been used.[16, 18-24] One versatile strategy used to prepared AuNPs is to use dendrimers as templates [25-27] or stabilizing agents.[28-30] Dendrimers are a class of highly branched, monodispersed, synthetic macromolecules with well defined structure and geometric architecture.[31-33] The branched internal cavity and modifiable functional periphery of dendrimers render the creation of dendrimer-entrapped AuNPs (Au DENPs) [15, 17, 34-36] and dendrimer-stabilized AuNPs (Au DSNPs) [37-41] with tunable functionalities for different CT imaging applications, especially for CT imaging of different types of cancer.[42-45] For instance, the periphery of generation 5 (G5) poly(amidoamine) (PAMAM) dendrimers can be modified with conventional iodine-based CT contrast agents, followed by entrapment of AuNPs within the dendrimer interior [46] or by stabilization of AuNPs on their surface[39] for enhanced CT imaging applications. Dendrimers pre-modified with targeting ligands (e.g., folic acid or lactobionic acid (LA)) can be used for further entrapment of AuNPs for targeted CT imaging of cancer.[42-45] These studies underline the important role played by dendrimers to form functionalized AuNPs for CT imaging applications.

For translational medicine applications of dendrimer-based AuNPs, it is necessary to avoid the use of commercially expensive high-generation dendrimers (G4 or above). Our

previous work has shown that a low-generation G2 PAMAM dendrimers can be used as either stabilizing agents to form Au DSNPs[37, 38] *via* a hydrothermal approach or as templates to form Au DENPs[47] *via* sodium borohydride reduction chemistry for CT imaging applications. In the latter process to generate Au DENPs, partial modification of the terminal amines of G2 dendrimers by polyethylene glycol (PEG) plays an important role to render the effective entrapment of AuNPs with a size of 2.8 nm. The PEGylation modification of dendrimer terminal amines is able to enlarge the dendrimer periphery, which is beneficial to not only render the entrapment of more Au within the dendrimer interior for high-generation dendrimers,[17, 41-43] but also afford the formation of stable Au DENPs for low-generation dendrimers.[47] With the versatile PEGylation conjugation chemistry that allows the convenient linking of targeting ligands on the one end of PEG segment,[43, 44] it is expected that Au DENPs formed using low-generation dendrimers are also able to be developed for targeted CT imaging of tumors.

In this present study, amine-terminated G2 PAMAM dendrimers ($G2.NH_2$) were first modified with fluorescein isothiocyanate (FI) and PEGylated LA. LA is known to be able to target hepatocellular carcinoma (HCC) overexpressing asialoglycoprotein receptors (ASGPR).[43, 48] The formed multifunctional G2 dendrimers were then employed as templates to form Au DENPs (Scheme 1). The formed LA-targeted Au DENPs (LA-Au DENPs) were characterized *via* different techniques. The cytotoxicity of the Au DENPs was evaluated by cell viability assay. The targeting specificity of the particles was assessed by flow cytometry *in vitro*. Next, the multifunctional LA-Au DENPs were used as a probe for CT imaging of HepG2 cells (an HCC cell line) *in vitro* and the xenografted tumor model *in vivo*. Finally, the long-term organ toxicity of the probe was evaluated *via* histological studies of the major organs after intravenous injection. To our knowledge, this is the first report related to the development of low-generation Au DENPs for targeted CT imaging of tumors.

Experimental

Materials

Ethylenediamine core $G2.NH_2$ PAMAM dendrimers were purchased from Dendritech (Midland, MI). FI and LA were obtained from Aldrich (St. Louis, MO). Chloroauric acid was from Sinopharm Chemical Reagent Co., Ltd (Shanghai, China). N-Hydroxysuccinimide (NHS) was from GL Biochem Ltd. (Shanghai, China). PEG with a carboxyl group at one end and an amine group at the other end (NH_2-PEG-COOH, Mw = 2 000) and PEG monomethyl ether with a carboxyl group at the other end (*m*PEG-COOH, Mw = 2 000) were supplied by Shanghai Yanyi Biotechnology Corporation (Shanghai, China). 1-Ethyl-3-(3-dimethylaminopropyl) carbodiimide hydrochloride (EDC) was acquired from J&K Chemical Reagent Co., Ltd (Shanghai, China). Cellulose dialysis membranes with molecular weight cut-offs (MWCOs) of 1 000 and 14 000 were acquired from Shanghai Yuanye Biotechnology Corporation (Shanghai, China). HepG2 cells were from Institute of Biochemistry and Cell Biology, the Chinese Academy of Sciences (Shanghai, China). Minimum Essential Medium (MEM) and fetal bovine serum (FBS) were purchased from Hangzhou Jinuo Biomedical Technology (Hangzhou, China) and Shanghai Excell Biology, Inc. (Shanghai, China), respectively. 3-(4, 5-Dimethylthiazol-2-yl)-2, 5-diphenyltetrazolium bromide (MTT) was acquired from Shanghai Sangon Biological Engineering Technology&Services Co., Ltd (Shanghai, China). Water used in all experiments was purified using a Milli-Q Plus 185 water purification system (Millipore, Bedford, MA) with a resistivity higher than 18.2 MΩ·cm.

Synthesis of multifunctional FI- and LA-modified G2 dendrimers

In brief, FI (26.28 μmol) dissolved in 25 mL dimethyl sulfoxide (DMSO) was added into a DMSO solution of $G2.NH_2$ (7.51 μmol, 25 mL) under vigorous magnetic stirring. After 24 h, the reaction mixture was extensively dialyzed against water (6 times, 2 L) using a dialysis membrane with an MWCO of 1 000 for 3 days, followed by lyophilization to get the $G2.NH_2$-FI product.

LA-PEG-COOH was synthesized according to protocols described in our previous reports.[43, 49] In brief, LA (135.16 μmol) dissolved in NaH_2PO_4-Na_2HPO_4 buffer (pH = 6.0, 0.02 M, 5.8 mL) was added with equal molar equivalent of EDC and NHS. The mixture was stirred for 3 h to activate the carboxyl group of LA. Then the activated LA was dropwise added to a NaH_2PO_4-Na_2HPO_4 buffer solution containing NH_2-PEG-COOH (90.10 μmol, 18 mL) and the mixture was stirred for 3 days. After that, the reaction mixture was extensively dialyzed against water (6 times, 2 L) using a dialysis membrane with an MWCO of 1 000 for 2 days, and then lyophilized to obtain the LA-PEG-COOH product.

The formed $G2.NH_2$-FI dendrimers were conjugated with LA-PEG-COOH *via* an EDC coupling reaction. Briefly, LA-PEG-COOH (86.91 μmol) dissolved in DMSO (14 mL) was first activated by equal molar equivalent of EDC with vigorous magnetic stirring for 6 h. Then, the activated LA-PEG-COOH was dropwise added to the DMSO solution of the $G2.NH_2$-FI dendrimer (5.79 μmol, 50 mL) under magnetic stirring for 3 days. The reaction mixture was then dialyzed against water (6 times, 2 L) using a dialysis membrane with an MWCO of 14 000 for 2 days, followed by lyophilization to obtain the $G2.NH_2$-FI-PEG-LA product. For comparison, $G2.NH_2$-FI-*m*PEG conjugate without LA was also prepared under similar conditions except the use of *m*PEG-COOH.

Synthesis of multifunctional LA-modified Au DENPs

The formed $G2.NH_2$-FI-PEG-LA dendrimers were used as templates to synthesize Au DENPs *via* sodium borohydride reduction chemistry with the dendrimer/gold salt molar ratio at 1/8, which is similar to our previous study.[47] Briefly, an $HAuCl_4$ aqueous solution (23.12 μmol, 400 μL) were added into an aqueous solution of $G2.NH_2$-FI-PEG-LA (2.89 μmol, 9 mL) under vigorous magnetic stirring. After 10 min, an icy cold aqueous solution of $NaBH_4$ (115.88 μmol, 440 μL) was added to the reaction mixture under stirring for 2 h. The reaction mixture changed from yellow to deep brown within a few seconds after addition of the $NaBH_4$ solution. The raw product of the Au DENPs was dialyzed against phosphate buffered saline (PBS, 3 times, 2 L) and water (3 times, 2 L) for 2 days using a dialysis membrane with an MWCO of 14 000, followed by lyophilization to get the $\{(Au^0)_8$-$G2.NH_2$-FI-PEG-LA$\}$ DENPs (for short, LA-

Au DENPs). For comparison, the non-targeted product of the {$(Au^0)_8$-G2.NH_2-FI-*m*PEG} DENPs (for short, nonLA-Au DENPs) was also prepared under similar experimental conditions.

Characterization techniques

^{1}H NMR spectra were recorded on a Bruker Avance 400 nuclear magnetic resonance spectrometer. Samples were dissolved in D_2O before measurements. UV-vis spectra were collected using a Lambda 25 UV-vis spectrophotometer (Perkin-Elmer, Boston, MA). Samples were dissolved in water before experiments. TEM was performed using a JEOL 2010F analytical electron microscope with an accelerating voltage of 200 kV. An aqueous solution of a sample (5 μL, 0.5 mg mL^{-1}) was dropped onto a carbon-coated copper grid and air dried before measurements. The size distribution histogram of each sample was measured using Image J software (http://rsb.info.nih.gov/ij/download.html). For each sample, 300 NPs were randomly selected from different images to analyze the size. ζ-potential and dynamic light scattering (DLS) measurements were performed using a Malvern Zetasizer Nano ZS model ZEN3600 (Worcestershire, UK) equipped with a standard 633 nm laser.

The stability of the LA-Au DENPs under different pH and temperature conditions was assessed by UV-vis spectroscopy. The samples were dispersed in NaH_2PO_4-Na_2HPO_4 buffer under different pHs (pH 5-8) and maintained for 20 min before measurements. In addition, the LA-Au DENPs dispersed in water were kept at different temperatures (4, 20, 37, and 50 °C, respectively) for 30 min before measurements. For comparison, G2.NH_2-FI dendrimer was also tested to illustrate the change of the FI-associated absorption feature under different conditions.

X-ray attenuation measurements

LA-Au DENPs or Omnipaque (300 mg I mL^{-1}, GE Healthcare, used as control) solutions with Au or iodine concentration in a range of 0-80 mM were prepared in 1.5-mL Eppendorf tubes and placed in a self-designed scanning holder. CT scans were performed using a clinical Brilliance 64-slice CT imaging system (Philips Healthcare, Andover, MA) with 120 kV, 200 mA, and a slice thickness of 1.5 mm. Evaluation of X-ray attenuation intensity was carried out by loading the digital CT images in a standard display program and then selecting a uniform round region of interest on the resultant CT image for each sample. The CT contrast enhancement was evaluated in Hounsfield units (HU) for each concentration of the LA-Au DENPs or Omnipaque.

Cell culture

HepG2 cells were continuously cultured and passaged in MEM supplemented with 10% FBS and 1% penicillin-streptomycin at 37 °C and 5% CO_2 in a humidified incubator.

Cytocompatibility assay

MTT assay was used to quantify the viability of HepG2 cells treated with the LA-Au DENPs and nonLA-Au DENPs at different concentrations. Briefly, 1×10^4 HepG2 cells were seeded into each well of a 96-well plate. After overnight incubation to bring the cells to about 80% confluence, the medium was replaced with fresh medium containing the LA-Au DENPs or nonLA-Au DENPs with concentrations ranging from 0 to 3000 nM, respectively. After 24 h incubation at 37 °C and 5% CO_2, MTT in PBS solution was added to each well to have a final concentration of 0.5 mg mL^{-1} and the cells were incubated for additional 4 h. The assays were carried out according to the manufacturer's instructions using a Thermo Scientific Multiskan MK3 ELISA reader (Thermo Scientific, Hudson, NH) at 570 nm. Mean and standard deviation for the quadruplicate wells were reported for each sample.

Flow cytometry

HepG2 cells were seeded in 24-well plates at a density of 2×10^5 cells/well. After overnight culture to bring the cells to confluence, the medium was replaced with fresh medium containing the LA-Au DENPs with concentrations ranging from 0 to 1000 nM. For comparison, nonLA-Au DENPs were also tested under similar experimental conditions. After 4 h incubation, the cells were washed with PBS for 3 times, trypsinized, resuspended in 0.5 mL PBS, and analyzed using a Becton Dickinson FACSCalibur flow cytometer.

***In vitro* CT imaging of human hepatocellular carcinoma**

HepG2 cells were cultured in a 6-well plate at a density of 1.5×10^6 cells/well one day prior to the experiment. Then the cell culture medium was replaced with fresh medium containing LA-Au DENPs with different concentrations (200, 500, 1000, 2000, and 3000 nM, respectively) and the cells were incubated for additional 4 h at 37 °C and 5% CO_2. NonLA-Au DENPs with the same concentrations were also tested for comparison. After washed with PBS for 3 times, the cells were trypsinized, centrifuged, and resuspended within 100 μL PBS in 0.5-mL Eppendorf tubes. The tubes were placed in a self-designed scanning holder and the cell suspensions were scanned using the same CT imaging system described above with 120 kV, 200 mA, and a slice thickness of 0.625 mm.

***In vivo* CT imaging of a xenografted tumor model**

All animal experiments were carried out following the protocols approved by the Ethical Committee of Shanghai First People's Hospital and the policy of the National Ministry of Health. For *in vivo* CT imaging, nude mice models grafted with Human HCC (20-25 g, subcutaneous injection of HepG2 cells) were purchased from Shanghai Rochen Biotech Co., Ltd (Shanghai, China). The tumor nodules had a volume of 0.4-0.9 cm^3. Each nude mouse was anesthetized by intraperitoneal injection of 1% pentobarbital sodium (4 mL/kg). LA-Au DENPs dispersed in PBS ([Au] = 0.05 M, 100 μL) were then intravenously injected into mice *via* tail vein. Omnipaque ([I] = [Au]) and nonLA-Au DENPs with a similar dose were also injected for comparison. The tumor-bearing nude mice were scanned using the above CT imaging system with the following operating parameters: tube voltage, 100 kV; tube current, 200 mA; and slice thickness, 0.625 mm.

***In vivo* biodistribution**

The tumor-bearing mice were intravenously injected with LA-Au DENPs ([Au] = 0.05 M, 100 μL in PBS) *via* tail vein. At 2 h, 24 h, and 48 h postinjection, the mice were euthanized. Then, the heart, liver, spleen, lung, kidney, and tumor were extracted and weighed. The organs were incubated in *aqua regia* solution for one day. The Au content was determined by inductively coupled plasma-optical emission spectroscopy (ICP-OES, Varian 710-ES,

Palo Alto, CA). To compare the difference in the Au uptake between the LA-Au DENPs and nonLA-Au DENPs, at 2 h postinjection of the LA-Au DENPs and nonLA-Au DENPs, the organs and the tumor tissue from the tumor-bearing mice were extracted and the Au uptake was quantified in a similar way.

Histological examinations

To further confirm the pathological impact of the Au DENPs on different organs, two healthy male 4- to 6- week-old BALB/C nude mice without tumor (Shanghai Slac Laboratory Animal Center, Shanghai, China) were used. One of them was intravenously injected with the LA-Au DENPs ([Au] = 0.05 M, 100 μL in PBS) *via* tail vein. After one month, the mouse was sacrificed. Then the heart, lung, liver, spleen, and kidney were harvested and fixed in 10% buffered formalin solution for 24 h. Then the organs were dehydrated, embedded with paraffin, and sectioned to have a thickness of 3 μm using a conventional microtome. The sections were then dewaxed, washed thoroughly with PBS, followed by hematoxylin & eosin (H&E) staining according to protocols reported in the literature.[44] Finally, each section was dehydrated and mounted onto a glass cover slip before optical microscopic observation. For comparison, the organs from the other untreated healthy mouse were treated similarly and were used as control.

Statistical analysis

One-way analysis of variance (ANOVA) statistical method was performed to evaluate the experimental data. A value of 0.05 was selected as the statistical significance level and the data were indicated with (*) for $p < 0.05$, (**) for $p < 0.01$, and (***) for $p < 0.001$, respectively.

Results and discussion

Synthesis and characterization of LA-Au DENPs

Previous work has shown that NPs modified with LA are able to target HCC.[43, 48] Therefore, in this study, we attempted to modify PEGylated LA onto the surface of G2 PAMAM dendrimers in order to render the subsequently formed Au DENPs with targeting specificity to HCC.

PEGylated LA (LA-PEG-COOH) was first synthesized and characterized by ^{1}H NMR (Figure S1b, Electronic Supplementary Information, ESI). The peak at around 3.7 ppm attributed to the -CH_2- protons of PEG and the proton peaks in the range of 3.8 to 4.3 ppm assigned to the LA moieties clearly suggest the successful formation of LA-PEG-COOH. Based on the NMR integration data, the number of LA moieties conjugated to each PEG molecule was calculated to be around 0.8. Before conjugation of LA-PEG-COOH on the G2 dendrimer surface, FI was initially modified onto the surface of G2 dendrimers in order to monitor the cellular uptake of the finally formed Au DENPs *via* flow cytometry. As shown in the ^{1}H NMR spectrum (Figure S1a, ESI), the proton signals in the range of 2.0-3.7 ppm are assigned to the -CH_2- protons of G2 dendrimers, while the proton peaks in the range of 6-8 ppm are associated to the FI moieties. This suggests the successful conjugation of FI moieties onto the surface of G2 dendrimers. By comparison of the NMR integration, the number of FI moieties attached to each G2 dendrimer was estimated to be 2.5. After that, LA-PEG-COOH was modified onto the surface of G2.NH_2-FI dendrimer *via* an EDC coupling reaction to synthesize the G2.NH_2-FI-PEG-LA conjugate. By comparison of the NMR integration of the PEG -CH_2- peak and the dendrimer -CH_2- peaks, the number of the LA-PEG moieties attached to each G2 dendrimer was calculated to be 6.0 (Figure S1c, ESI). For comparison, the control conjugate of G2.NH_2-FI-*m*PEG without LA was also prepared and the number of *m*PEG attached to each G2 dendrimer was estimated to be 6.1 based on the NMR integration data (Figure S1d, ESI). The conjugation of FI onto the G2 dendrimers can also be verified by UV-vis spectroscopy (Figure 1). The peak at 500 nm for the G2.NH_2-FI, G2.NH_2-FI-PEG-LA, and G2.NH_2-FI-*m*PEG conjugates is typical for the absorption feature of the attached FI moiety.

The synthesized G2.NH_2-FI-PEG-LA and G2.NH_2-FI-*m*PEG dendrimers were then used as templates to form AuNPs. The formation of AuNPs can be visually confirmed by the color change of the dendrimer solution after sodium borohydride reduction reaction (Figure 1, inset). It can be seen that G2.NH_2-FI displays a deep orange color, and the further conjugation of PEG-LA or *m*PEG lightens the orange color of the dendrimer solution. After the formation of AuNPs, both LA-Au DENPs and nonLA-Au DENPs display a deep brown color. UV-vis spectrometry was also used to prove the successful formation of AuNPs (Figure 1). It can be seen that the absorption of the attached FI moiety is overlapped with the typical surface plasmon resonance (SPR) band of AuNPs, similar to our previous studies.[30, 43] However, after the formation of AuNPs, a strong build up appeared in the range of 500-800 nm for both LA-Au DENPs and nonLA-Au DENPs, which is attributed to the NP-resulted light scattering effect.

The existence of AuNPs was further confirmed by TEM imaging (Figure 2). It is clear that the LA-Au DENPs exhibit a spherical shape with quite a narrow size distribution. The mean Au core size was estimated to be 1.8 nm (Figure 2a). High-resolution TEM image reveals that the AuNPs entrapped within the G2 dendrimers are highly crystalline as lattices can be clearly observed (Figure 2a, inset). The control Au DENPs without LA modification display a similar morphology, crystal structure, and size distribution (Figure 2b). This suggests that the PEGylation modification of G2 dendrimer periphery regardless of the LA modification is powerful to render the formation of AuNPs within the dendrimer interior, in agreement with our previous work.[47] The PEGylation modification (Mw of PEG = 2 000) of G2 dendrimers with a size of 2.9 nm is believed to largely extend the dendrimer periphery,[50] enabling effective entrapment of AuNPs with a size of 1.8 nm. In this context, formation of Au DSNPs is unlikely possible. Through DLS, the hydrodynamic size of the formed LA-Au DENPs and nonLA-Au DENPs was measured to be 480.5 ± 57.0 nm and 471.5 ± 74.0 nm, respectively (Table S1, ESI). The measured hydrodynamic sizes are much larger than those measured by TEM. This is because DLS measures the size of large aggregates or clusters of particles in aqueous solution, while TEM just measures single Au core NPs.[37, 43]

The surface potentials of the LA-Au DENPs and the nonLA-Au DENPs were measured to be +6.6 and + 6.3 mV, respectively (Table S1, ESI). It seems that the PEGylation modification of the G2 dendrimers is able to largely shield the positive surface

potential of the particles, which is important to endow the particles with improved cytocompatibility. In this case, similar to our previous study,[10] no additional acetylation of the remaining dendrimer terminal amines is required.

Stability of LA-Au DENPs

The stability of Au DENPs is important for their further biomedical imaging applications. We checked the stability of the LA-Au DENPs under different temperature and pH conditions *via* UV-vis spectrometry (Figures S2 and S3, ESI), since the aggregation state of the AuNPs can be directly reflected by the changes of their SPR bands under different conditions. Our results reveal that no apparent SPR band shifting occurs when the particles are dispersed in water at the temperature of 4, 20, 37, and 50 ^{o}C, respectively (Figure S2, ESI). Likewise, the LA-Au DENPs have increased absorbance at 500 nm with the increase of the solution pH (Figure S3a, ESI), which is similar to the G2.NH_2-FI conjugate in the absence of AuNPs (Figure S3b, ESI). The increased absorbance of FI moiety with pH may be due to the change of the protonation state of FI moieties (pKa of FI = 6.4). It is known that the absorbance of deprotonated FI is higher than that of protonated FI (http://en.wikipedia.org/wiki/Fluorescein). This implies that the absorption feature of the entrapped AuNPs does not have any significant changes, and the entrapped AuNPs are stable under different pH conditions. The stability of the LA-Au DENPs was also checked by dispersing them in water, PBS, and cell culture medium. We show that the particles are colloidally stable and no precipitation occurs after the particles were stored at room temperature for one month. The nonLA-Au DENPs basically display the same stability as the LA-Au DENPs (Figure S4, ESI).

Cytocompatibility assay

We next explored the cytocompatibility of both LA-Au DENPs and nonLA-Au DENPs at different concentrations *via* MTT cell viability assay (Figure 3). MTT assay data show that the viability of HepG2 cells slightly decreases with the increase of the particle concentration, and the cell viability remains 80% or above even when the particle concentration is up to 3000 nM. Moreover, it can be seen that the LA-Au DENPs display approximately similar cytotoxicity to the nonLA-Au DENPs. This suggests that the developed Au DENPs with or without LA modification are quite cytocompatible, which is essential for their biomedical applications.

Flow cytometry

Flow cytometry was used to assess the targeting specificity of the developed LA-Au DENPs by monitoring the FI-related green fluorescence in the cells. The nonLA-Au DENPs without LA were also tested for comparison (Figure 4). Due to the non-specific cellular uptake of NPs *via* phagocytosis and diffusion *via* cell membranes,[35, 51] the cellular uptake of both particles increased with the concentration. However, under similar particle concentrations, the fluorescence intensity of cells treated with the LA-Au DENPs was significantly higher than that of cells treated with the nonLA-Au DENPs ($p < 0.001$). This should be attributed to LA-mediated targeting of the particles to ASGPR-overexpressing HepG2 cells.

X-ray attenuation measurements

Prior to apply the developed LA-Au DENPs for targeted CT imaging of cancer cells, the X-ray attenuation property of the particles was investigated (Figure 5). For comparison, Omnipaque, an iodinated small molecular CT contrast agent was also tested. Visually, the brightness of CT images for both LA-Au DENPs and Omnipaque is enhanced with the radiodense element concentration (Au or I). Under the same concentration of Au or I (0.04 M or above), the CT image of LA-AuDENPs is brighter than that of Omnipaque (Figure 5a). This was further proven by quantitative analysis of CT values (Figure 5b). The X-ray attenuation intensity of both the LA-Au DENPs and Omnipaque increased with the molar concentration of Au or I, and the increasing trend of the LA-Au DENPs is much higher than that of Omnipaque. It should be noted that the used Au or I concentration range and CT imaging time are quite similar to those reported in our previous work.[17, 43, 49] This ensures the reasonable comparison. The better X-ray attenuation property of the LA-Au DENPs than that of Omnipaque is beneficial for them to be used in more sensitive CT imaging applications.

Targeted CT imaging of cancer cells *in vitro*

We then used the developed LA-Au DENPs as a nanoprobe for targeted CT imaging of HepG2 cells *in vitro*. The nonLA-Au DENPs without LA were also tested for comparison (Figure 6). It can be seen that in both cases, the cell CT value increases with the particle concentration. Under the same Au concentration, the CT value of cells treated with the LA-Au DENPs is significantly higher than that treated with the nonLA-Au DENPs ($p < 0.001$). This again suggests the role played by the LA-mediated targeting that enables enhanced and specific CT imaging of HepG2 cells overexpressing ASGPR, corroborating the flow cytometry data.

Targeted CT imaging of a xenografted tumor model *in vivo*

The feasibility to use the LA-Au DENPs as a probe for targeted CT imaging of a xenografted HepG2 tumor model *in vivo* was next explored (Figure 7, and Figure S5, ESI). The transectional (Figure 7a) and coronal (Figure S5) tumor CT images were collected and the CT values of the tumor region were quantified before and at different time points post intravenous injection of the LA-Au DENPs. The nonLA-Au DENPs and Omnipaque were also injected for comparison. It is clear that at 20 min postinjection, the CT value of the Omnipaque group starts to descend, while those of both Au DENPs still continue to increase till 90 min. Apparently, under the same time point, both Au DENPs display much higher CT values than Omnipaque, which is due to the better X-ray attenuation property of Au DENPs than that of Omnipaque. Likewise, the fast metabolism of Omnipaque makes it rapidly be cleared and therefore Omnipaque is unable to image tumors for a long time period. In contrast, the nanoscale size of the developed Au DENPs renders them with extended blood circulation time, thereby enabling CT imaging of tumors in an extended time period *via* enhanced permeability and retention (EPR) effect. More importantly, the tumor CT values after injection of the LA-Au DENPs were much higher than those after injection of the nonLA-Au DENPs at the same time point post intravenous injection. At 90 min postinjection, the tumor CT value of the non-targeted group leveled off, while the tumor CT

value of the targeted one still displayed a dramatic increase. Our results suggest that besides the passive tumor targeting *via* EPR effect, the LA-mediated active targeting enables the LA-Au DENPs to have enhanced and extended accumulation in the tumor site, thereby allowing for targeted and enhanced tumor CT imaging.

In vivo biodistribution

The biodistribution of Au element in tumor tissue and several major organs (heart, lung, spleen, liver, kidney, tumor, and blood) was studied by ICP-OES at 2 h post intravenous injection of both LA-Au DENPs and nonLA-Au DENPs (Figure 8). It can be observed that for both non-targeted and targeted Au DENPs, spleen has the maximum Au uptake, followed by the liver and kidney. This implies that the PEGylated Au DENPs with or without LA modification are able to escape the reticuloendothelial system (RES) and pass through the renal filtration. What' more, compared with the nonLA-Au DENPs, the LA-Au DENPs appeared to have less tendency to be accumulated in the other major organs, but have more uptake in the tumor site. This further demonstrated the specific LA-mediated active targeting role. The metabolism of the LA-Au DENPs after intravenous injection was further investigated in an extended time period (Figure S6, ESI). It can be seen that after 24 h, the Au uptake in all the organs starts to descend, suggesting that the developed nanoprobe is able to be metabolized and cleared out from the body. This is very important for its practical biomedical imaging applications.

Histological studies

In order to evaluate the long-term organ compatibility, one healthy BALB/C nude mouse intravenously injected with the LA-Au DENPs was sacrificed at one month postinjection. The major organs including the liver, lung, spleen, heart, and kidney were extracted, sectioned, and H&E stained before histological examinations (Figure 9). Clearly, compared to the control group without injection of Au DENPs, the morphology of all the studied organs did not seem to have appreciable changes. This suggests that the intravenously injected LA-Au DENPs ([Au] =0.05 M, 100 μL) do not display apparent *in vivo* toxicity to the organs.

Conclusion

In summary, we demonstrated a facile approach to synthesizing LA-modified Au DENPs using G2 dendrimers pre-modified with PEG as templates for targeted tumor CT imaging applications. The covalent modification of PEGylated LA onto the surface of amine-terminated G2 PAMAM dendrimers not only allows the dendrimers to be used as templates for effective entrapment of AuNPs with a core size of 1.8 nm, but also enables the formed Au DENPs with targeting specificity to ASGPR-overexpressing cancer cells. The developed LA-Au DENPs are water-dispersible, colloidally stable under different pH and temperature conditions, and non-cytotoxic in the given concentration range. More importantly, the LA-Au DENPs can be used as an efficient nanoprobe for targeted CT imaging of HepG2 cells *in vitro* and the xenografted tumor model *in vivo* thanks to the LA-mediated active targeting. The developed Au DENPs using PEGylated low generation dendrimers as templates may hold great promise to be used as nanoprobes for CT imaging of different types of cancer.

Acknowledgements

This research is financially supported by the National Natural Science Foundation of China (81351050, 81101150, and 21273032), the Fund of the Science and Technology Commission of Shanghai Municipality (12520705500), the Ph.D. Programs Foundation of Ministry of Education of China (20130075110004), and the Program for Professor of Special Appointment (Eastern Scholar) at Shanghai Institutions of Higher Learning.

Notes and references

[a] *State Key Laboratory for Modification of Chemical Fibers and Polymer Materials, College of Materials Science and Engineering, Donghua University, Shanghai 201620, People's Republic of China.*

[b] *Department of Radiology, Shanghai Songjiang District Central Hospital, Shanghai 201600, People's Republic of China. E-mail: xiajd_21@s163.com*

[c] *College of Chemistry, Chemical Engineering and Biotechnology, Donghua University, Shanghai 201620, People's Republic of China. E-mail: xshi@dhu.edu.cn*

[§] These authors equally contributed to this work.

† **Electronic supplementary information (ESI) available**: additional experimental results.

1. H. Lusic and M. W. Grinstaff, *Chem. Rev.*, 2012, **113**, 1641-1666.
2. F. Hyafil, J.-C. Cornily, J. E. Feig, R. Gordon, E. Vucic, V. Amirbekian, E. A. Fisher, V. Fuster, L. J. Feldman and Z. A. Fayad, *Nat. Med.*, 2007, **13**, 636-641.
3. C. Haller and I. Hizoh, *Invest. Radiol.*, 2004, **39**, 149-154.
4. K. Ai, Y. Liu, J. Liu, Q. Yuan, Y. He and L. Lu, *Adv. Mater.*, 2011, **23**, 4886-4891.
5. Y. Fang, C. Peng, R. Guo, L. Zheng, J. Qin, B. Zhou, M. Shen, X. Lu, G. Zhang and X. Shi, *Analyst*, 2013, **138**, 3172-3180.
6. J. M. Kinsella, R. E. Jimenez, P. P. Karmali, A. M. Rush, V. R. Kotamraju, N. C. Gianneschi, E. Ruoslahti, D. Stupack and M. J. Sailor, *Angew. Chem. Int. Ed.*, 2011, **50**, 12308-12311.
7. O. Rabin, J. M. Perez, J. Grimm, G. Wojtkiewicz and R. Weissleder, *Nat. Mater.*, 2006, **5**, 118-122.
8. Z. Liu, E. G. Ju, J. H. Liu, Y. D. Du, Z. Q. Li, Q. H. Yuan, J. S. Ren and X. G. Qu, *Biomaterials*, 2013, **34**, 7444-7452.
9. Z. Liu, K. Dong, J. Liu, X. Han, J. Ren and X. Qu, *Small*, 2014, **10**, 2429-2438.
10. Z. Liu, F. Pu, J. H. Liu, L. Y. Jiang, Q. H. Yuan, Z. Q. Li, J. S. Ren and X. G. Qu, *Nanoscale*, 2013, **5**, 4252-4261.
11. Y. Liu, K. Ai, J. Liu, Q. Yuan, Y. He and L. Lu, *Angew. Chem. Int. Ed.*, 2012, **51**, 1437-1442.
12. M. H. Oh, N. Lee, H. Kim, S. P. Park, Y. Piao, J. Lee, S. W. Jun, W. K. Moon, S. H. Choi and T. Hyeon, *J. Am. Chem. Soc.*, 2011, **133**, 5508-5515.
13. P. A. Jackson, W. N. W. Abd Rahman, C. J. Wong, T. Ackerly and M. Geso, *Eur. J. Radiol.*, 2010, **75**, 104-109.
14. J. F. Hainfeld, D. N. Slatkin, T. M. Focella and H. M. Smilowitz, *Br. J. Radiol.*, 2006, **79**, 248-253.
15. R. Guo, H. Wang, C. Peng, M. Shen, M. Pan, X. Cao, G. Zhang and X. Shi, *J. Phys. Chem. C*, 2010, **114**, 50-56.
16. D. Kim, S. Park, J. H. Lee, Y. Y. Jeong and S. Jon, *J. Am. Chem. Soc.*, 2007, **129**, 7661-7665.
17. C. Peng, L. F. Zheng, Q. Chen, M. W. Shen, R. Guo, H. Wang, X. Y. Cao, G. X. Zhang and X. Y. Shi, *Biomaterials*, 2012, **33**, 1107-1119.
18. N. S. Md, H.-K. Kim, J.-A. Park, Y. Chang and T.-J. Kim, *Bull. Korean Chem. Soc.*, 2010, **31**, 1177-1181.
19. I.-C. Sun, D.-K. Eun, J. H. Na, S. Lee, I.-J. Kim, I.-C. Youn, C.-Y. Ko, H.-S. Kim, D. Lim, K. Choi, P. B. Messersmith, T. G. Park, S. Y.

Kim, I. C. Kwon, K. Kim and C.-H. Ahn, *Chem.-Eur. J.*, 2009, **15**, 13341-13347.
20. E.-K. Lim, E. Jang, J. Kim, T. Lee, E. Kim, H. S. Park, J.-S. Suh, Y.-M. Huh and S. Haam, *J. Mater. Chem.*, 2012, **22**, 17518-17524.
21. W. Eck, A. I. Nicholson, H. Zentgraf, W. Semmler and S. Bartling, *Nano Lett.*, 2010, **10**, 2318-2322.
22. Y. Jin, J. Wang, H. Ke, S. Wang and Z. Dai, *Biomaterials*, 2013, **34**, 4794-4802.
23. V. Kattumuri, K. Katti, S. Bhaskaran, E. J. Boote, S. W. Casteel, G. M. Fent, D. J. Robertson, M. Chandrasekhar, R. Kannan and K. V. Katti, *Small*, 2007, **3**, 333-341.
24. N. Chanda, R. Shukla, A. Zambre, S. Mekapothula, R. R. Kulkarni, K. Katti, K. Bhattacharyya, G. M. Fent, S. W. Casteel, E. J. Boote, J. A. Viator, A. Upendran, R. Kannan and K. V. Katti, *Pharm. Res.*, 2011, **28**, 279-291.
25. X. Shi, S. Wang, S. Meshinchi, M. E. Van Antwerp, X. Bi, I. Lee and J. R. Baker, Jr., *Small*, 2007, **3**, 1245-1252.
26. X. Shi, S. Wang, H. Sun and J. R. Baker, *Soft Matter*, 2007, **3**, 71-74.
27. R. Shukla, E. Hill, X. Shi, J. Kim, M. C. Muniz, K. Sun and J. R. Baker, Jr., *Soft Matter*, 2008, **4**, 2160-2163.
28. X. Shi, T. R. Ganser, K. Sun, L. P. Balogh and J. R. Baker, Jr, *Nanotechnology*, 2006, **17**, 1072-1078.
29. X. Shi, K. Sun and J. R. Baker, Jr., *J. Phys. Chem. C*, 2008, **112**, 8251-8258.
30. X. Shi, S. H. Wang, M. E. Van Antwerp, X. Chen and J. R. Baker, Jr., *Analyst*, 2009, **134**, 1373-1379.
31. D. A. Tomalia and J. M. J. Frechet, *Dendrimers and Other Dendritic Polymers*, John Wiley & Sons Ltd, New York, 2001.
32. L. M. Bronstein and Z. B. Shifrina, *Chem. Rev.*, 2011, **111**, 5301-5344.
33. M. A. Mintzer and M. W. Grinstaff, *Chem. Soc. Rev.*, 2011, **40**, 173-190.
34. C. Peng, H. Wang, R. Guo, M. W. Shen, X. Y. Cao, M. F. Zhu, G. X. Zhang and X. Y. Shi, *J. Appl. Polym. Sci.*, 2011, **119**, 1673-1682.
35. H. Wang, L. Zheng, C. Peng, R. Guo, M. Shen, X. Shi and G. Zhang, *Biomaterials*, 2011, **32**, 2979-2988.
36. T. Xiao, S. Wen, H. Wang, H. Liu, M. Shen, J. Zhao, G. Zhang and X. Shi, *J. Mater. Chem. B*, 2013, **1**, 2773-2780.
37. H. Liu, Y. Xu, S. Wen, Q. Chen, L. Zheng, M. Shen, J. Zhao, G. Zhang and X. Shi, *Chem.-Eur. J.*, 2013, **19**, 6409-6416.
38. H. Liu, Y. Xu, S. Wen, J. Zhu, L. Zheng, M. Shen, J. Zhao, G. Zhang and X. Shi, *Polym. Chem.*, 2013, **4**, 1788-1795.
39. C. Peng, K. Li, X. Cao, T. Xiao, W. Hon, L. Zheng, R. Guo, M. Shen, G. Zhang and X. Shi, *Nanoscale*, 2012, **4**, 6768-6778.
40. H. Liu, M. Shen, J. Zhao, J. Zhu, T. Xiao, X. Cao, G. Zhang and X. Shi, *Analyst*, 2013, **138**, 1979-1987.
41. S. Wen, K. Li, H. Cai, Q. Chen, M. Shen, Y. Huang, C. Peng, W. Hou, M. Zhu, G. Zhang and X. Shi, *Biomaterials*, 2013, **34**, 1570-1580.
42. Q. Chen, K. Li, S. Wen, H. Liu, C. Peng, H. Cai, M. Shen, G. Zhang and X. Shi, *Biomaterials*, 2013, **34**, 5200-5209.
43. H. Liu, H. Wang, Y. Xu, R. Guo, S. Wen, Y. Huang, W. Liu, M. Shen, J. Zhao, G. Zhang and X. Shi, *ACS Appl. Mater. Interfaces*, 2014, **6**, 6944-6953.
44. C. Peng, J. Qin, B. Zhou, Q. Chen, M. Shen, M. Zhu, X. Lu and X. Shi, *Polym. Chem.*, 2013, **4**, 4412-4424.
45. H. Wang, L. Zheng, C. Peng, M. Shen, X. Shi and G. Zhang, *Biomaterials*, 2013, **34**, 470-480.
46. R. Guo, H. Wang, C. Peng, M. Shen, L. Zheng, G. Zhang and X. Shi, *J. Mater. Chem.*, 2011, **21**, 5120-5127.
47. H. Liu, H. Wang, Y. Xu, M. Shen, J. Zhao, G. Zhang and X. Shi, *Nanoscale*, 2014, **6**, 4521-4526.
48. R. Guo, Y. Yao, G. Cheng, S. H. Wang, Y. Li, M. Shen, Y. Zhang, J. R. Baker, Jr., J. Wang and X. Shi, *RSC Adv.*, 2012, **2**, 99-102.
49. F. Fu, Y. Wu, J. Zhu, S. Wen, M. Shen and X. Shi, *ACS Appl. Mater. Interfaces*, 2014, **6**, 16416-16425.
50. G. M. Pavan, A. Barducci, L. Albertazzi and M. Parrinello, *Soft Matter*, 2013, **9**, 2593-2597.
51. H. Yang, C. Zhang, X. Shi, H. Hu, X. Du, Y. Fang, Y. Ma, H. Wu and S. Yang, *Biomaterials*, 2010, **31**, 3667-3673.

Figure captions

Scheme 1. Schematic illustration of the synthesis of LA-PEG-COOH segment, LA-Au DENPs, and nonLA-Au DENPs.

Figure 1. UV-vis spectra of G2.NH_2-FI (1), G2.NH_2-FI-PEG-LA (2), G2.NH_2-FI-*m*PEG (3), {$(Au^0)_8$-G2.NH_2-FI-PEG-LA} DENPs (4), and {$(Au^0)_8$-G2.NH_2-FI-*m*PEG} DENPs (5). Inset shows the picture of the aqueous solution of the corresponding materials.

Figure 2. TEM images and size distribution histograms of (a) {$(Au^0)_8$-G2.NH_2-FI-PEG-LA} DENPs and (b) {$(Au^0)_8$-G2.NH_2-FI-*m*PEG} DENPs. Insets in both (a) and (b) show the high-resolution TEM image of the respective particles.

Figure 3. MTT viability assay of HepG2 cells treated with the LA-Au DENPs or non-LA Au DENPs for 24 h. The cells treated with PBS were used as control. The data were expressed as mean ± S.D (n = 3).

Figure 4. Flow cytometry analysis of HepG2 cells after treatment with the LA-Au DENPs or non-LA Au DENPs for 4 h. The cells treated with PBS were used as control. The data were expressed as mean ± S.D (n = 3).

Figure 5. CT images (a) and X-ray attenuation intensity (HU) (b) of (1) Omnipaque and (2) LA-Au DENPs with different concentrations of radiodense element (Au or iodine). In (a), the numbers on the left represent the Au or iodine concentrations (M) for the LA-Au DENPs or Omnipaque.

Figure 6. CT images (a) and X-ray attenuation intensity (HU) (b) of HepG2 cells treated with (1) LA-Au DENPs and (2) nonLA-Au DENPs with different concentrations. In (a), the numbers on the left represent the particle concentrations (nM).

Figure 7. (a) Transectional CT images of the HepG2 tumor model before and after intravenous

injection of Omnipaque, LA-Au DENPs, and nonLA-Au DENPs, respectively. The yellow arrows point to the tumor area. (b) The corresponding CT values of the tumor area after different treatments at different time points.

Figure 8. *In vivo* biodistribution of Au element in different organs and tumor at 2 h postinjection of the LA-Au DENPs and nonLA-Au DENPs ([Au] = 0.05 M, in 100 μL PBS).

Figure 9. HE staining of the sections of the liver, lung, spleen, heart, and kidney in a healthy nude mouse at one month post intravenous injection of the LA-Au DENPs. Organs from the other untreated mouse were used as control.

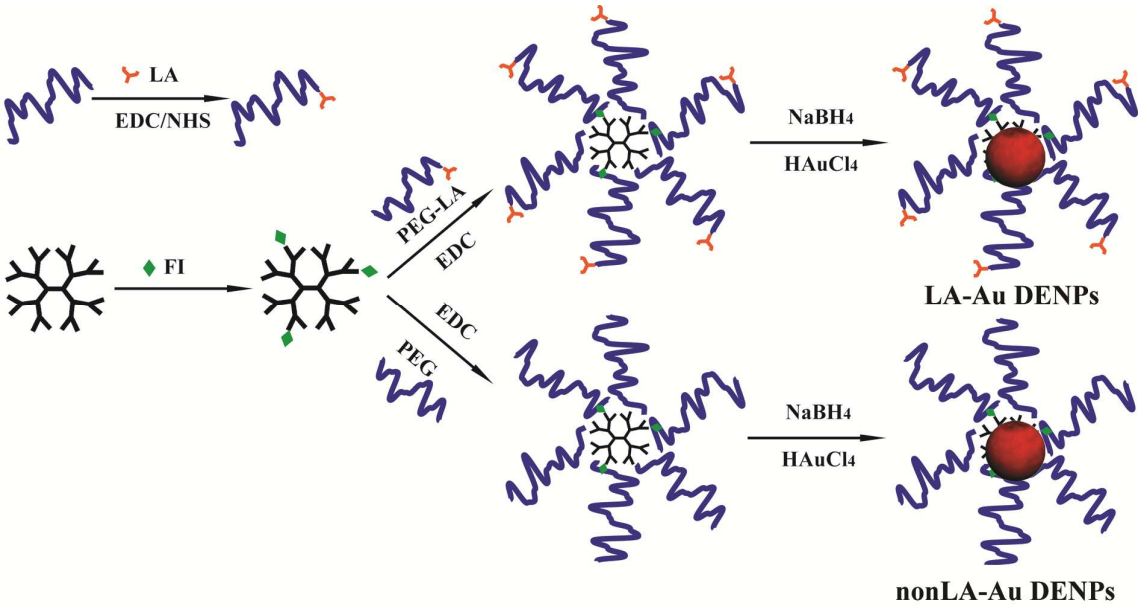

Scheme 1

Cao *et al.*

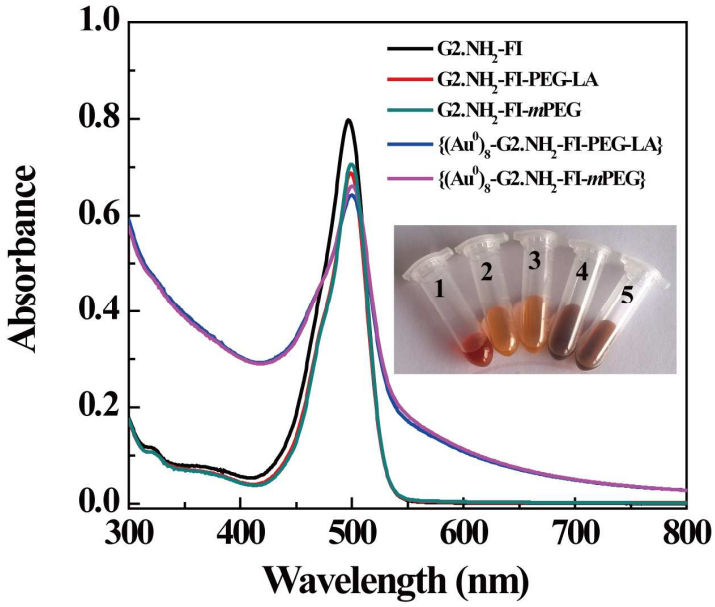

Figure 1

Cao *et al.*

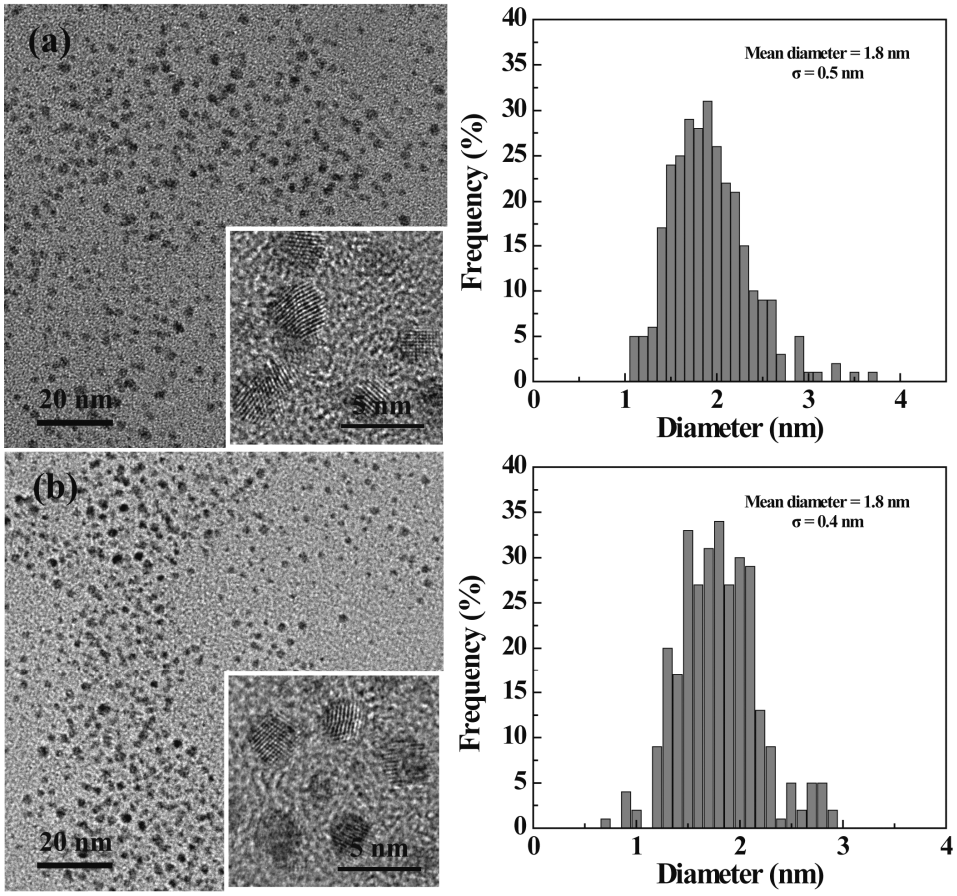

Figure 2

Cao *et al.*

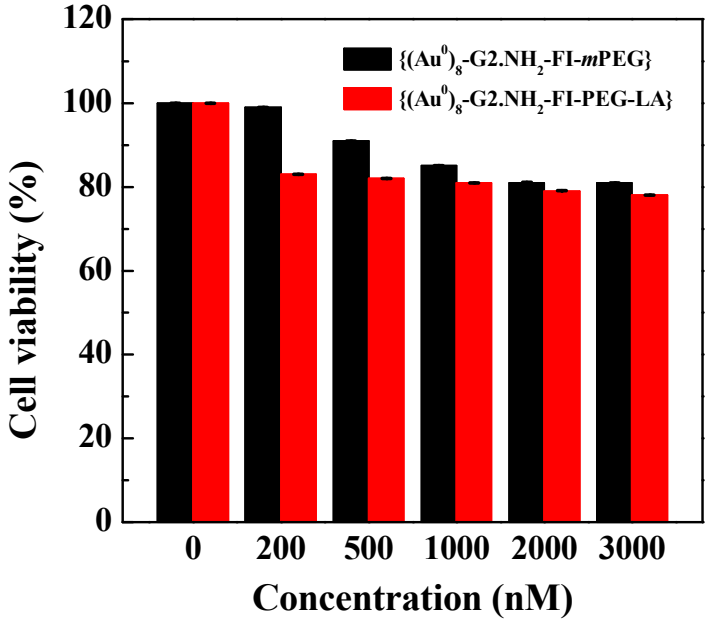

Figure 3

Cao *et al.*

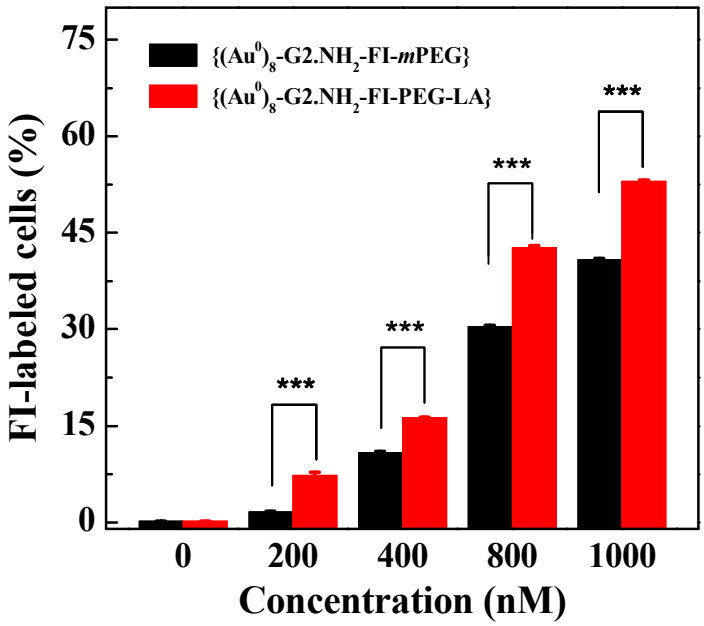

Figure 4

Cao *et al.*

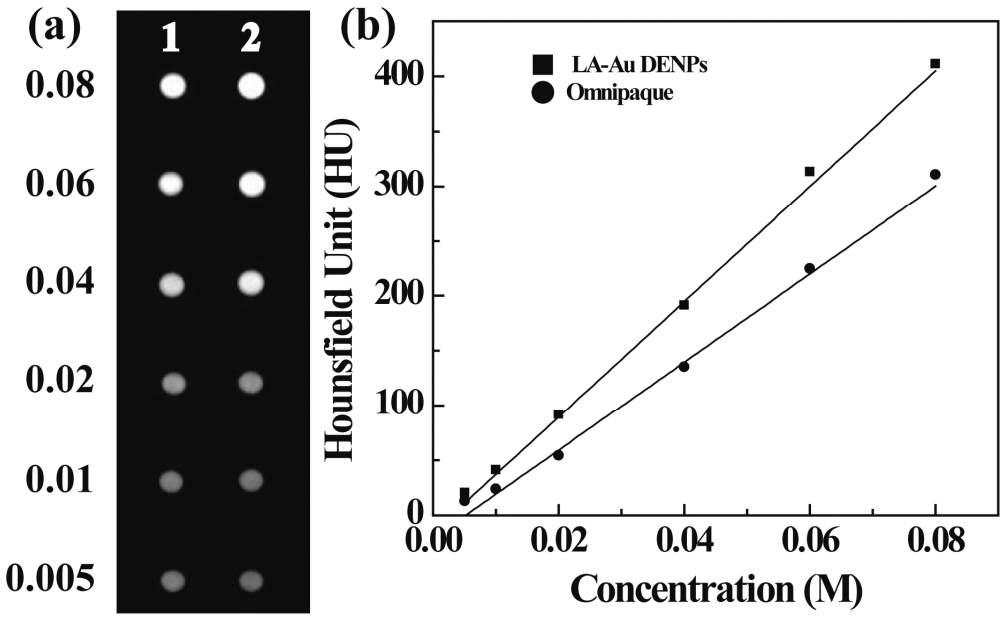

Figure 5

Cao *et al.*

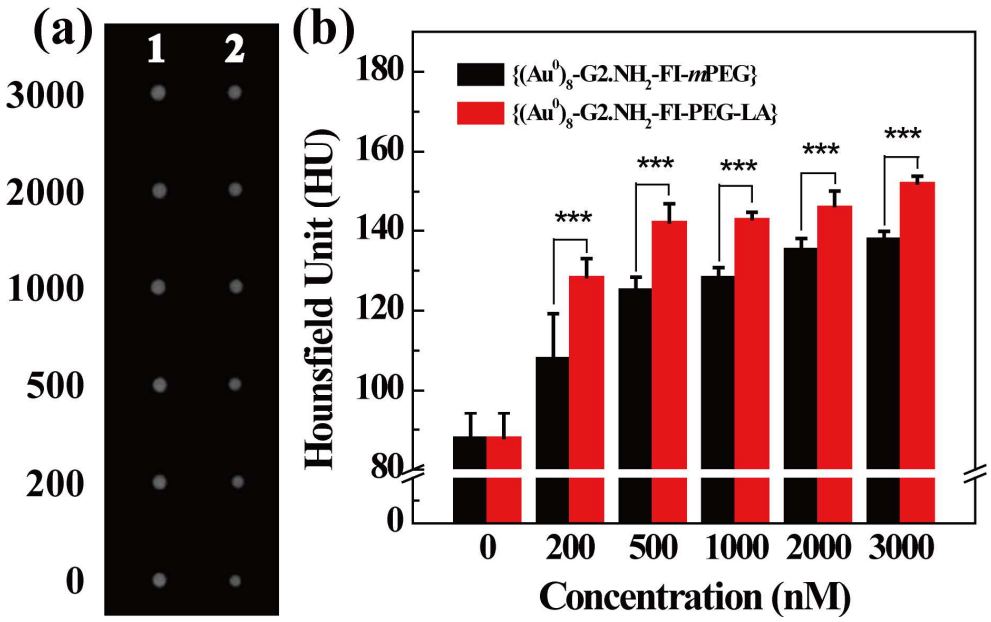

Figure 6

Cao *et al.*

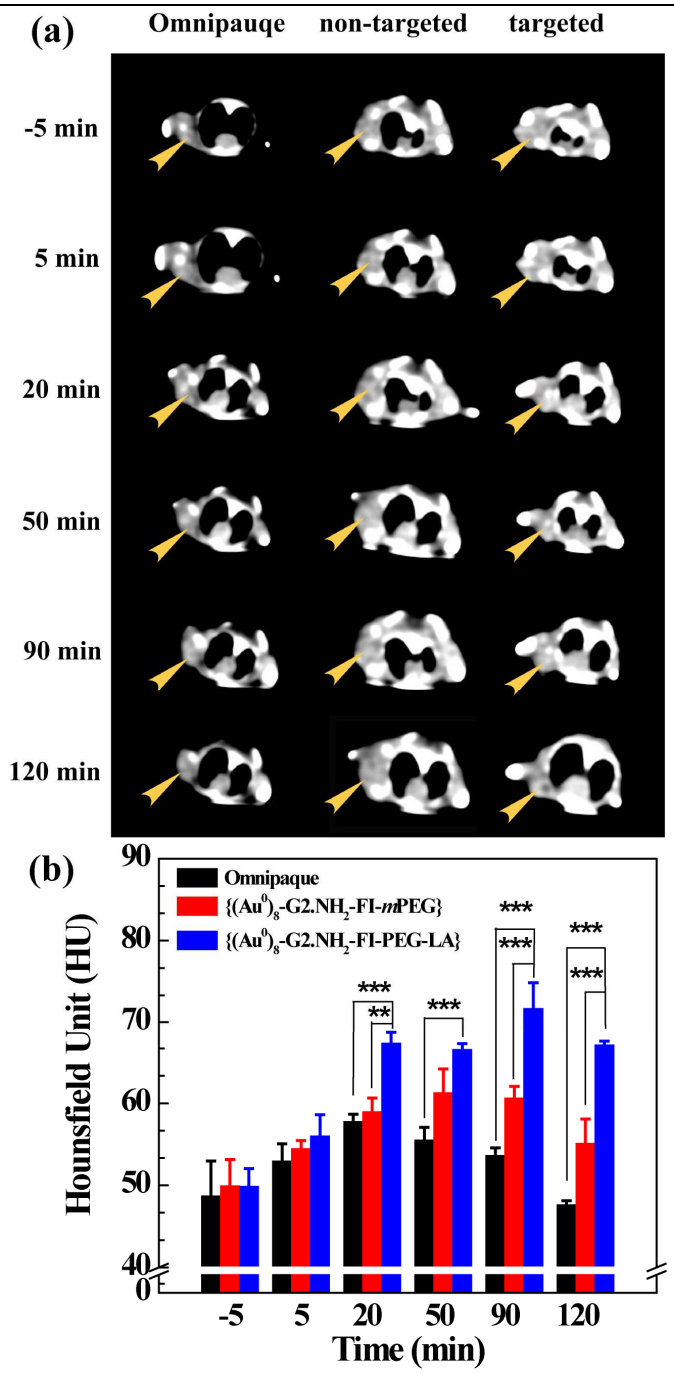

Figure 7

Cao *et al.*

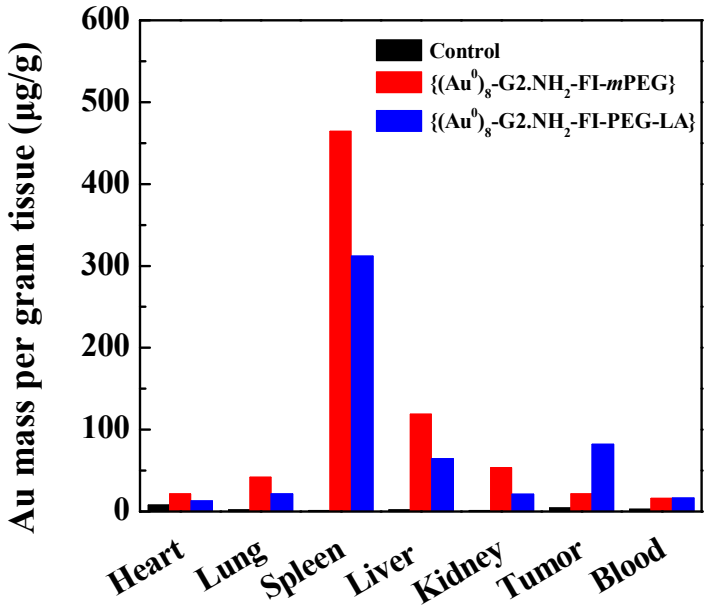

Figure 8

Cao *et al.*

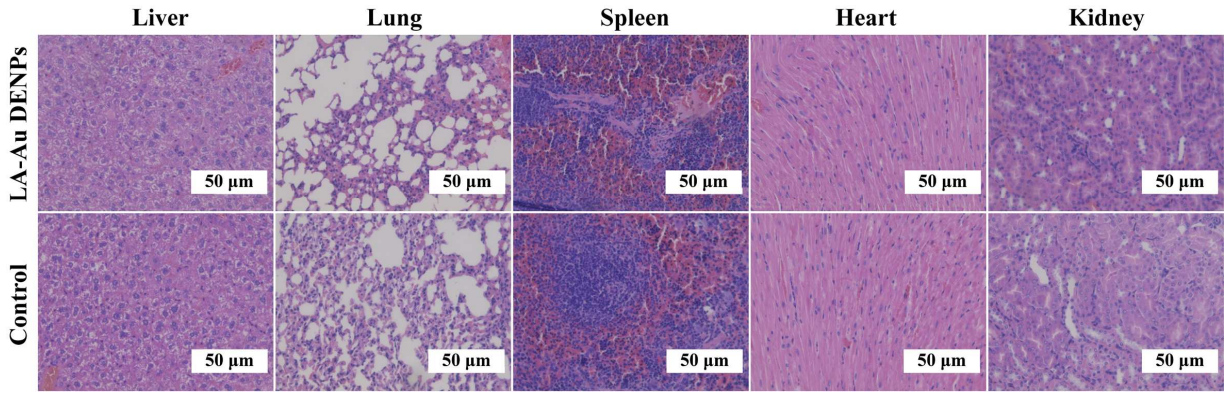

Figure 9

Cao *et al.*

Table of Contents (TOC) Image

Targeted CT imaging of human hepatocellular carcinoma using low-generation dendrimer-entrapped gold nanoparticles modified with lactobionic acid†

Yiyun Cao,[a§] Yao He,[b§] Hui Liu,[c] Yu Luo,[c] Mingwu Shen,[c] Jindong Xia,*[b] Xiangyang Shi*[ac]

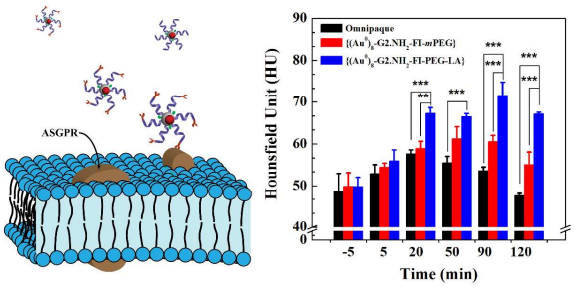

Dendrimer-entrapped gold nanoparticles formed using low-generation dendrimers modified with PEGylated lactobionic acid as templates enable targeted CT imaging of human hepatocellular carcinoma.